

Application of the Finite-Element-with-Discontinuous-Support Method to Thermal Radiation Transport

Andrew Till,* Robert Lowrie,* Christopher Fontes†

*CCS-2: Computational Physics and Methods Group, Los Alamos National Laboratory, P.O. Box 1663, Los Alamos, NM

†XCP-5: Materials and Physical Data Group, Los Alamos National Laboratory, P.O. Box 1663, Los Alamos, NM
till@lanl.gov, lowrie@lanl.gov, cjf@lanl.gov

Abstract - Previous work has developed the Finite-Element-with-Discontiguous Support (FEDS) method for discretizing the energy variable for neutron transport (NT) using discontinuous and discontinuous finite elements in energy. Like nuclear cross sections for NT, atomic opacities in thermal radiation transport (TRT) exhibit rapid oscillations as a function of particle energy. These oscillations are difficult to treat numerically with the popular multigroup (MG) discretization when the number of degrees of freedom (DOF) in energy (the number of groups) is much less than the number of lines, which is often the case. These interaction similarities motivate us to apply the FEDS method to TRT problems. We derive FEDS for TRT and compare with MG as a function of number of DOF in energy for a wall-heating problem, finding FEDS often is more consistently convergent and has lower error than MG for the same number of DOF.

I. INTRODUCTION

Thermal radiation transport (TRT) shares numerous physical and computational similarities with neutron transport (NT). Both describe the advection and interaction of neutral particles through and with a medium. The solution to the TRT equations consists of the angular intensity and temperature at all times for all spatial locations, all photon directions, and all photon energies.¹ Like the angular flux for NT, the TRT angular intensity lives in a six-dimensional phase space plus time. The interaction of the radiation with matter is characterized by nuclear cross sections for NT and atomic opacities for TRT. Both exhibit rapid oscillatory behavior as a function of particle energy. In NT, this is due to resonances from quantized nuclear energy levels of the compound nucleus, while in TRT it is due to lines and edges from excitation and ionization of the bound electrons. Figure 1 gives the absorption attenuation coefficients² for the CRASH-like problem defined and studied in future sections.

To the extent that TRT is similar to NT, the same discretization methods should be effective for both. In this work, we focus on discretization in energy, noting that while some NT codes do employ continuous-in-energy cross sections, few TRT codes do. The most popular energy discretization method for both TRT and NT is the multigroup (MG) method, which combines particles with similar energies and solves for the sum of their intensity using group-averaged opacities.

MG can be sensitive to approximations in the weighting spectrum chosen for opacity averaging, especially in the common case where groups span many lines or edges. As a result, MG often inaccurately treats important phenomena such as self-shielding variations. From a finite-element viewpoint,

¹We distinguish the energy of an individual photon, which is directly proportional to its frequency, from the energy in the photon field, which we call the intensity. "Photon energies" refers to the former.

²The attenuation coefficient (1/cm), also known as an inverse mean-free-path, is the product of the corresponding opacity (cm²/g) and the mass density (g/cm³). Another name for the opacity is the mass attenuation coefficient. The absorption attenuation coefficient is sometimes called absorbtivity while the total attenuation coefficient is sometimes called the extinction coefficient.

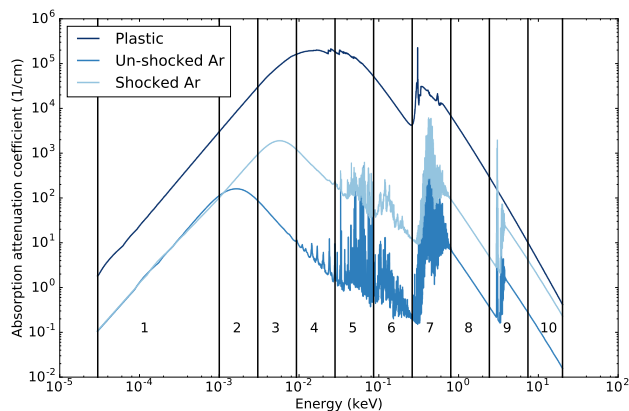


Fig. 1: Energy-dependent absorption attenuation coefficients for the CRASH-like problem along with coarse group boundaries and numbers.

MG uses a single fixed basis function (the pre-selected spectrum) within each group, with no mechanism to adapt to local solution behavior.

In previous work [1, 2], the Finite-Element-with-Discontiguous-Support (FEDS) method was applied to NT. We showed that, for FEDS, errors in reaction-rate based quantities of interest, including the criticality eigenvalue, decreased with increasing numbers of energy unknowns in the energy range with resolved resonances, but not so for MG when groups did not resolve the resonances. We were able to achieve 50×10^{-5} relative error in all resonance coarse groups for all nuclide reaction rates with 225 energy unknowns in the resolved resonance region. We demonstrated that using S_N in conjunction with FEDS is a powerful method for solving realistic NT problems at high resolution.

In this paper, we extend the FEDS method to TRT. We begin by noting relevant differences between TRT and NT. We then review the finite-element underpinnings of FEDS, introduce basis function definitions specific to TRT, and derive the FEDS TRT equations. We briefly describe how to generate energy meshes for FEDS. Next, we compare FEDS to MG

as a function of number of energy unknowns (i.e., degrees of freedom [DOFs] in energy) for a simplified semi-analytic model. We conclude by looking ahead to extensions that may be required to make FEDS performant for TRT problems with large temperature ranges, many partially ionized materials, and varying densities.

II. THEORY

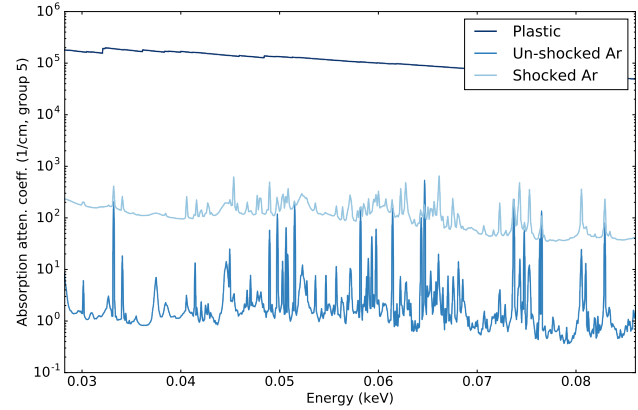
1. Relevant Differences Between TRT and NT

Aspects of TRT and its opacities create unique numerical challenges. The main challenge involves increased dimensionality of the atomic opacities used in TRT compared to the nuclear cross sections used in NT. The essential difference is that the nuclear cross sections at different temperatures are highly correlated whereas the atomic opacities are partially correlated at different temperature and density states. By correlation we mean, for a given photon energy, being able to predict the opacity at one temperature / density from the opacity at a different temperature / density.

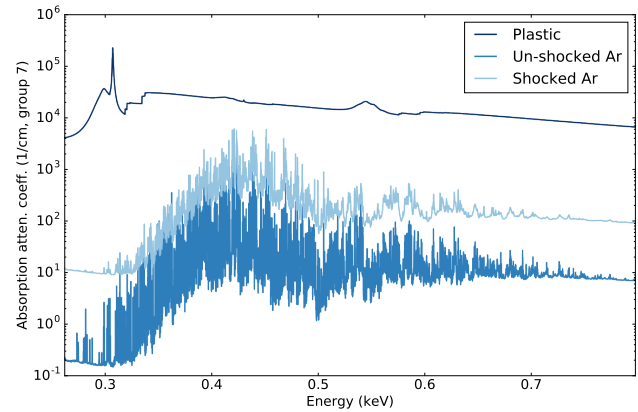
Were the opacities at different temperatures / densities perfectly correlated, it would be accurate to use a multiband or ODF (opacity distribution function) method [3].³ The totally un-correlated case would similarly be straightforward to treat, for example by using multiband with an interface conditions to smear the intensity within a group over its bands when going to a cell with a non-correlated opacity. Partial correlation is difficult to treat because such interface conditions are not analytic.

Figure 2 zooms in on two energies ranges to show the line structure of some opacities. While the argon opacities at the two temperature-density points share many lines, the magnitudes of the lines differ in complicated ways. Figure 3 shows the same data differently. Instead of plotting two lines of opacity vs energy, for each photon energy in the dataset a mark is added to the plot with x -position corresponding to the opacity for one state of argon and the y -position corresponding to the opacity for the other state. This comparison shows the correlation between the two opacities. Similarity occurs because disparate opacities share terms in the sum over atomic cross sections (cm^2), and because the atomic cross sections for different ion stages represent lines and edges at similar locations. However, due to difference in ion stage populations, not all lines are present at every temperature and density, and those that are shared may be present in differing proportion. This behavior explains the imperfect correlation of the argon opacities in Fig. 3, with perfect correlation corresponding to all of the data lying on one line and correlation decreasing with increasing data spread.

FEDS worked well for NT because the solution was low-dimensional. It was able to be represented with relatively few DOFs in energy, each of which was an energy element that lived within discontinuous energy ranges. An important cause of this low dimensionality was few important resonant nuclides. For many TRT problems, there are many important opacities because each temperature/density point acts as a new



(a) Fifth coarse group



(b) Seventh coarse group

Fig. 2: Energy-dependent absorption attenuation coefficients for two energies ranges of the CRASH-like problem.

material whose opacity has its own fine structure.

Despite these differences, we extend FEDS to TRT, beginning with a conceptually simple but numerically challenging problem that highlights the potential and challenges for FEDS. Future work will look at generalizing FEDS while maintaining its strengths of consistency of correlations among differing materials / temperatures / densities and accuracy / convergence, even at low DOFs in energy.

2. The FEDS Method for TRT

The FEDS method is a Petrov-Galerkin finite-element method. Our weight functions, $w_e(E)$ for element index $e \in \{1, \dots, N_e\}$, are unity for energies within an energy element and zero otherwise. The basis functions have the same support as the weight functions but also have a normalized spectral shape. The “DS” in FEDS indicates that the weight and basis functions are allowed to have discontinuous support. We require that elements do not overlap, which gives us weight and basis functions that are orthonormal. Our FEDS angular

³See [1] for a history, literature review, and comparison of different energy discretization methods.

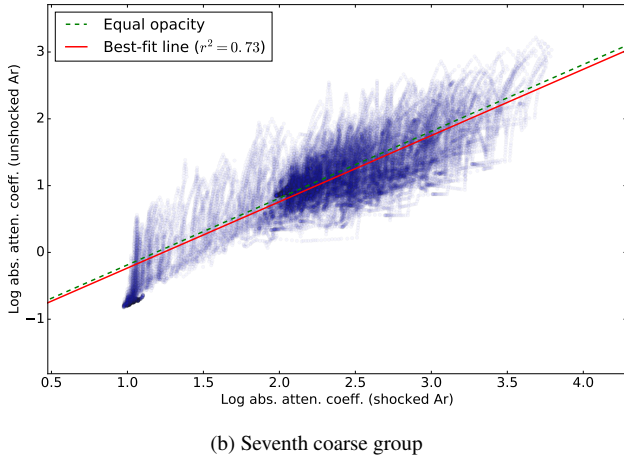
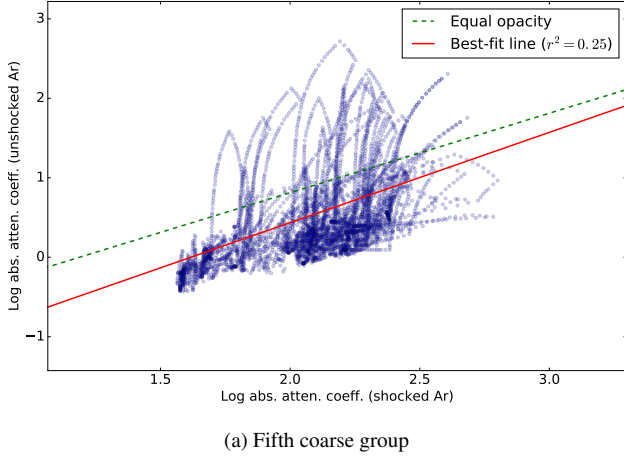


Fig. 3: Comparison of absorption attenuation coefficients for two energy ranges between un-shocked and shocked argon for the CRASH-like problem. The log of the attenuation coefficients are plotted against each other for each datapoint. Each blue dot corresponds to a different photon energy. The green dashed line indicates where the data would lie if the two argon states had the same opacities. The solid red line is a linear best-fit to the data.

intensity solution is defined as a basis function expansion:

$$I(\mathbf{r}, E, \boldsymbol{\Omega}, t) = \sum_e b_e(\mathbf{r}, E, t) I_e(\mathbf{r}, \boldsymbol{\Omega}, t), \quad (1)$$

where \mathbf{r} is location (cm), E is photon energy (keV), $\boldsymbol{\Omega}$ is photon direction, t is time (s), I is the energy-dependent angular intensity ($\text{erg/cm}^2\text{-s-ster-keV}$), I_e is the angular intensity integrated over element e ($\text{erg/cm}^2\text{-s-ster}$), and the basis functions, $b_e(\mathbf{r}, E, t)$ (1/keV), often have a spatial and temporal dependence on the local temperature and/or density. Equation (1) is the only approximation for FEDS applied to NT. For TRT, in addition to the basis function expansion, we make two, similar approximations, described below.

We now introduce basis functions that produce flat-, Planck- and Rosseland-averaged opacities. Unnormalized examples of the latter weighting functions are given in Fig. 4.

Flat weighting implies $b_e(\mathbf{r}, E, t)$ is constant in energy within an element. To produce Planck-averaged opacities, we use a basis function that is the Planckian at the local material temperature:

$$b_{e,p}(\mathbf{r}, E, t) = \frac{B(T_m(\mathbf{r}, t), E) w_e(E)}{\int_0^\infty dE B(T_m(\mathbf{r}, t), E) w_e(E)}, \quad (2a)$$

$$B(T, E) = \frac{2}{h^3 c^2} \frac{E^3}{e^{E/T} - 1}, \quad (2b)$$

$$\int_{4\pi} d\boldsymbol{\Omega} \int_0^\infty dE B(T, E) = acT^4, \quad (2c)$$

where T_m is the local electron temperature (keV), $B(T, E)$ is the Planck function ($\text{erg/cm}^2\text{-s-ster-keV}$), c is the speed of light (cm/s), h is the Planck constant (keV/Hz), and a is the radiation constant ($\text{erg/cm}^3\text{-keV}^4$).

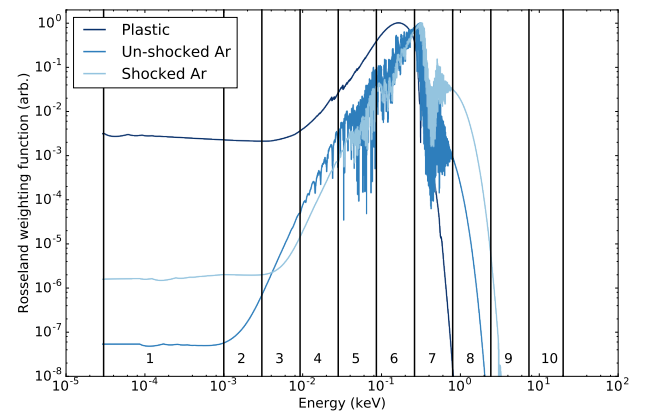
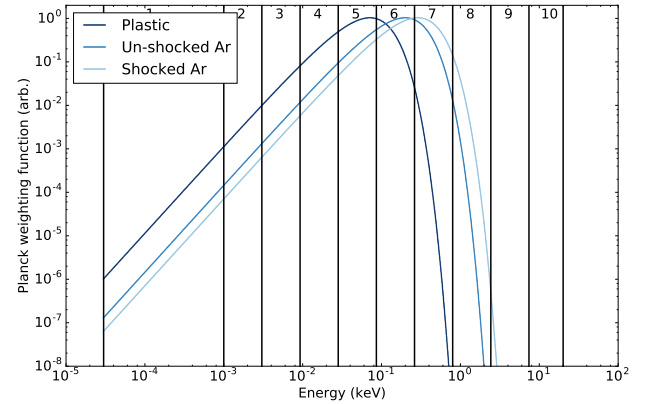


Fig. 4: Energy-dependent weighting functions for each material in the CRASH-like problem

To produce Rosseland-averaged opacities, we use a Rosseland-equivalent basis function of:

$$b_{e,R}(\mathbf{r}, E, t) = \frac{\left(\frac{\partial B}{\partial T} \frac{1}{\kappa_t}\right) w_e(E)}{\int_0^\infty dE \left(\frac{\partial B}{\partial T} \frac{1}{\kappa_t}\right) w_e(E)} \Big|_{(\rho_m(\mathbf{r},t), T_m(\mathbf{r},t))}, \quad (3a)$$

$$\frac{\partial B}{\partial T}(T, E) = \frac{2}{h^3 c^2} \frac{1}{T} \frac{E^3}{e^{E/T} - 1} \frac{E/T}{1 - e^{-E/T}}, \quad (3b)$$

where κ_t is the total opacity (cm²/g) and depends on the local density, ρ_m (g/cm³), and local electron temperature. The opacity is related to the absorption attenuation coefficient by the mass density: $\sigma_t = \rho_m \kappa_t$. Further discussion of Rosseland-weighted opacities are provided in the first appendix.

Under the assumption of local thermodynamic equilibrium (LTE), these averaged opacities depend upon T_m and ρ_m directly and \mathbf{r} and t only indirectly for single-material cells. The averaged opacities can be pre-computed on a native temperature-density grid and interpolated during run-time, as is typically done with MG opacities.

The continuous TRT equations are, assuming mono-energetic (Thomson) scattering:

$$\left(\frac{1}{c} \frac{\partial}{\partial t} + \mathbf{\Omega} \cdot \nabla + \sigma_t(\rho_m, T_m, E)\right) I(\mathbf{r}, E, \mathbf{\Omega}, t) = \frac{c}{4\pi} \sigma_s(\rho_m, T_m, E) \mathcal{E}(\mathbf{r}, E, t) + \sigma_a(\rho_m, T_m, E) B(T_m, E), \quad (4a)$$

$$C_v(\rho_m, T_m) \frac{\partial}{\partial t} T(\mathbf{r}, t) = \int_0^\infty dE \sigma_a(\rho_m, T_m, E) (c \mathcal{E}(\mathbf{r}, E, t) - 4\pi B(T_m, E)), \quad (4b)$$

$$\mathcal{E}(\mathbf{r}, E, t) \equiv \frac{1}{c} \int_{4\pi} d\mathbf{\Omega} I(\mathbf{r}, E, \mathbf{\Omega}, t), \quad (4c)$$

where \mathcal{E} is the radiation energy density (erg/cm³-keV), C_v is the specific heat⁴ (erg/cm³-keV), and σ_t , σ_a , and σ_s are the total, absorption, and scattering attenuation coefficients (1/cm), respectively.

Applying a backward Euler time discretization, we linearize the Planckian but lag the opacities:

$$\begin{aligned} & \left(\tau + \mathbf{\Omega} \cdot \nabla + \sigma_t(\rho^n, T^n, E)\right) I^{n+1}(\mathbf{r}, E, \mathbf{\Omega}) = \\ & \sigma_a(\rho^n, T^n, E) \left(B(T^n, E) + \frac{\partial B}{\partial T}(T^n, E) (T^{n+1} - T^n)\right) + \\ & \frac{c}{4\pi} \sigma_s(\rho^n, T^n, E) \mathcal{E}^{n+1}(\mathbf{r}, E) + \tau I^n(\mathbf{r}, E, \mathbf{\Omega}), \end{aligned} \quad (5a)$$

$$\begin{aligned} & c\tau C_v(\rho^n, T^n) (T^{n+1}(\mathbf{r}, t) - T^n(\mathbf{r})) = \\ & \int_0^\infty dE \sigma_a(\rho^n, T^n, E) c \mathcal{E}^{n+1}(\mathbf{r}, E) - \\ & \int_0^\infty dE 4\pi \sigma_a(\rho^n, T^n, E) \left(B(T^n, E) + \frac{\partial B}{\partial T}(T^n, E) (T^{n+1} - T^n)\right), \end{aligned} \quad (5b)$$

⁴ $C_v = \rho \hat{C}_v / k_B$, where k_B is Boltzmann's constant (8.617×10^{-8} keV/K) and \hat{C}_v is the more traditional specific heat in erg/g-K.

where $\tau = 1/(c\Delta t)$ in 1/cm, $\rho^n = \rho_m(\mathbf{r}, t^n)$, and $T^n = T_m(\mathbf{r}, t^n)$. For economy of notation, we simplify all lagged terms as, e.g., $\sigma_a^n(\mathbf{r}, E) = \sigma_a(\rho^n, T^n, E)$.

Defining

$$\chi^n(\mathbf{r}, E) \equiv \frac{\sigma_a^n(\mathbf{r}, E) \frac{\partial B^n}{\partial T}(\mathbf{r}, E)}{\int_0^\infty dE \sigma_a^n(\mathbf{r}, E) \frac{\partial B^n}{\partial T}(\mathbf{r}, E)}, \quad (6a)$$

$$\nu^n(\mathbf{r}) \equiv \frac{\int_0^\infty dE 4\pi \sigma_a^n(\mathbf{r}, E) \frac{\partial B^n}{\partial T}(\mathbf{r}, E)}{c\tau C_v^n(\mathbf{r}) + \int_0^\infty dE 4\pi \sigma_a^n(\mathbf{r}, E) \frac{\partial B^n}{\partial T}(\mathbf{r}, E)}, \quad (6b)$$

$$f^{n+1}(\mathbf{r}) \equiv \int_0^\infty dE \sigma_a^n(\mathbf{r}, E) c \mathcal{E}^{n+1}(\mathbf{r}, E), \quad (6c)$$

$$\begin{aligned} \xi^n(\mathbf{r}, E, \mathbf{\Omega}) & \equiv \tau I^n(\mathbf{r}, E, \mathbf{\Omega}) + \sigma_a^n(\mathbf{r}, E) B^n(\mathbf{r}, E) - \\ & \chi^n(\mathbf{r}, E) \nu^n(\mathbf{r}) \int_0^\infty dE \sigma_a^n(\mathbf{r}, E) B^n(\mathbf{r}, E), \end{aligned} \quad (6d)$$

the time-discretized TRT equations become:

$$\begin{aligned} & \left(\mathbf{\Omega} \cdot \nabla + (\sigma_t^n(\mathbf{r}, E) + \tau)\right) I^{n+1}(\mathbf{r}, E, \mathbf{\Omega}) = \\ & \frac{c}{4\pi} \sigma_s^n(\mathbf{r}, E) \mathcal{E}^{n+1}(\mathbf{r}, E) + \chi^n(\mathbf{r}, E) \nu^n(\mathbf{r}) f^{n+1}(\mathbf{r}) + \xi^n(\mathbf{r}, E, \mathbf{\Omega}), \end{aligned} \quad (7a)$$

$$T^{n+1} = T^n + \nu^n(\mathbf{r}) \frac{f^{n+1}(\mathbf{r}) - \int_0^\infty dE \sigma_a^n(\mathbf{r}, E) 4\pi B^n(\mathbf{r}, E)}{\int_0^\infty dE \sigma_a^n(\mathbf{r}, E) 4\pi \frac{\partial B^n}{\partial T}(\mathbf{r}, E)}. \quad (7b)$$

To derive the FEDS transport equation, (i) we take the time-discretized continuous-energy transport and material internal energy equations (Eq. (5)), (ii) expand the angular intensity and its integrals into their basis function expansions using Eq. (1), (iii) multiply the transport equation by the weight functions, and (iv) integrate over all energies. After some algebra, we arrive at an energy-discretized transport equation that is distinguishable from the MG transport equation only in the definition of the opacities, which are basis-function weighted, and the source, which now involves an integral over the discontinuous element. For further details, see below or [1].

The FEDS discretization of the time-discretized TRT equations becomes:

$$\begin{aligned} & \left(\mathbf{\Omega} \cdot \nabla + (\sigma_{t,e}^n(\mathbf{r}) + \tau)\right) I_e^{n+1}(\mathbf{r}, \mathbf{\Omega}) = \\ & \frac{c}{4\pi} \sigma_{s,e}^n(\mathbf{r}) \mathcal{E}_e^{n+1}(\mathbf{r}) + \chi_e^n(\mathbf{r}) \nu^n(\mathbf{r}) f^{n+1}(\mathbf{r}) + \xi_e^n(\mathbf{r}, \mathbf{\Omega}), \end{aligned} \quad (8a)$$

$$T^{n+1} = T^n + \nu^n(\mathbf{r}) \frac{f^{n+1}(\mathbf{r}) - \sum_e \sigma_{a,e}^n(\mathbf{r}) 4\pi B_e^n(\mathbf{r})}{\sum_e \sigma_{a,e}^n(\mathbf{r}) 4\pi \frac{\partial B_e^n}{\partial T}(\mathbf{r})}, \quad (8b)$$

where $\sigma_{a,e}$ is the basis-function-weighted absorption attenuation coefficient (1/cm; see above for definition of basis functions), and B_e is the Planck source integrated over an energy

element (erg/cm²-s-ster). Specifically,

$$\begin{aligned}\sigma_{x,e}^n(\mathbf{r}) &= \int_0^\infty dE b_e(\mathbf{r}, E, t) \sigma_x(\rho^n, T^n, E) \\ &= \frac{\int_{\Delta E_e} dE b_e(\mathbf{r}, E, t) \sigma_x(\rho^n, T^n, E)}{\int_{\Delta E_e} dE b_e(\mathbf{r}, E, t)},\end{aligned}\quad (9a)$$

$$\begin{aligned}B_e^n(\mathbf{r}) &= \int_0^\infty dE w_e(E) B(T^n, E) \\ &= \int_{\Delta E_e} dE B(T^n, E),\end{aligned}\quad (9b)$$

$$\begin{aligned}\frac{\partial B_e^n}{\partial T}(\mathbf{r}) &= \int_0^\infty dE w_e(E) \frac{\partial B}{\partial T}(T^n, E) \\ &= \int_{\Delta E_e} dE \frac{\partial B}{\partial T}(T^n, E),\end{aligned}\quad (9c)$$

$$\chi_e^n(\mathbf{r}) = \frac{\sigma_{a,e}^n(\mathbf{r}) \frac{\partial B_e^n}{\partial T}(\mathbf{r})}{\sum_k \sigma_{a,k}^n(\mathbf{r}) \frac{\partial B_k^n}{\partial T}(\mathbf{r})},\quad (9d)$$

$$\nu^n(\mathbf{r}) \equiv \frac{4\pi \sum_e \sigma_{a,e}^n(\mathbf{r}) \frac{\partial B_e^n}{\partial T}(\mathbf{r})}{c\tau C_v^n(\mathbf{r}) + 4\pi \sum_e \sigma_{a,e}^n(\mathbf{r}) \frac{\partial B_e^n}{\partial T}(\mathbf{r})},\quad (9e)$$

$$f^{n+1}(\mathbf{r}) \equiv \sum_e \sigma_{a,e}^n(\mathbf{r}) c\mathcal{E}_e^{n+1}(\mathbf{r}),\quad (9f)$$

$$\xi_e^n(\mathbf{r}, \mathbf{\Omega}) \equiv \tau I_e^n(\mathbf{r}, \mathbf{\Omega}) + \sigma_{a,e}^n(\mathbf{r}) B_e^n(\mathbf{r}) - \chi_e^n(\mathbf{r}) \nu^n(\mathbf{r}) \sum_k \sigma_{a,k}^n(\mathbf{r}) B_k^n(\mathbf{r}).\quad (9g)$$

Our two additional approximations for FEDS applied TRT are to equate

$$\int_0^\infty dE w_e(E) \sigma_a(\rho, T, E) B(T, E) \simeq \sigma_{a,e}(\rho, T) B_e(T),\quad (10a)$$

$$\int_0^\infty dE w_e(E) \sigma_a(\rho, T, E) \frac{\partial B}{\partial T}(T, E) \simeq \sigma_{a,e}(\rho, T) \frac{\partial B_e}{\partial T}(T),\quad (10b)$$

using basis-function weighting for the opacities instead of weighting with B or $\partial B/\partial T$. These approximations are often used with MG as well. The former approximation becomes exact if the basis functions are the Planck distribution at the local material temperature.

A primary difference from MG is that, for FEDS, ΔE_e is a discontinuous range of energies. Consequences of this difference are explored in the second appendix. We discuss how to generate this energy mesh in the next section.

3. Generating the Energy Mesh

The energy mesh describes the support of the weight and basis functions, with a function being nonzero for energies within an energy element and zero for energies outside an energy element. We assume we are given a library of spectra

and then solve a minimization problem by applying a clustering algorithm to these spectra. The output clusters define the energy mesh. We will describe one inexpensive way to generate approximate spectra.

When generating energy meshes, our MG implementation uses the typical even logarithmic spacing in energy between groups. FEDS first splits the entire energy range into multiple coarse groups, and then applies clustering to define elements separately in each coarse group. We use an equal number of elements per coarse group and fixed coarse group boundaries of 3.00×10^{-5} , 1.00×10^{-3} , 3.04×10^{-3} , 9.27×10^{-3} , 2.82×10^{-2} , 8.60×10^{-2} , 2.62×10^{-1} , 7.98×10^{-1} , 2.43, 7.40, and 20.0 keV. These boundaries are drawn in Figures 1 and 4.

Given spectra, we formulate and solve a minimization problem, so-named because its solution has minimized variance of the spectra within each energy element. The final energy mesh is defined so as to minimize the projection error of the spectra from their original resolved grid to this coarser grid. Our FEDS method, built on this energy mesh, can locally adapt to the true spectral behavior of the solution if the spectra well represent the solution and a sufficient number of DOFs are used. For more details on the solving the minimization problem with clustering, see [1].

We use the equilibrium diffusion limit (EDL) to motivate our spectra choice. In this limit, $I(E) \simeq B(T, E) - \frac{1}{\sigma_t(\rho, T, E)} \frac{\partial B}{\partial T}(T, E) \mathbf{\Omega} \cdot \nabla T$. Both B and $\partial B/\partial T$ are slowly varying in energy. We can either resolve them using the coarse group structure, or add $B(T, E)$ to the set of spectra we use. $\sigma_t(\rho, T, E)$ has both rapidly varying components from the lines and edges, and slowly varying components: free-free and bound-free (after the edge) interactions both scale as E^{-3} , while scattering off free electrons depends on the Klein-Nishina formula.

Assuming the slowly varying components in energy are resolved, we use spectra proportional to $1/\sigma_t(T_m, \rho_m, E)$ on a user-defined grid of temperatures, T_m , and densities, ρ_m . For TRT problems, the densities and materials are known ahead of time. For this paper, we assume the temperatures are also known ahead of time. Relaxing these limitations would be important for applying FEDS to realistic TRT problems.

Our minimization solver is not designed to handle spectra that vary by orders of magnitude. Instead, we take a logarithm of our spectra and use those. This means using σ_t or $1/\sigma_t$ for our spectra have the same result.

Figure 5 shows an example spectrum. For each coarse group, a separate application of a clustering algorithm on the spectra produces the FEDS energy mesh within that coarse group. In Fig. 5, colors are used to specify this full mesh, with each element corresponding to a different color. Energy elements may be discontinuous but are restricted to lie within one coarse group.

III. RESULTS AND ANALYSIS

We present a simplified CRASH-like [4] problem that consists of a single intensity characteristic in a time-independent setting. We fix the temperatures and densities, which linearizes the problem, and use a blackbody radiation source. The problem is meant to simulate experiments where laser

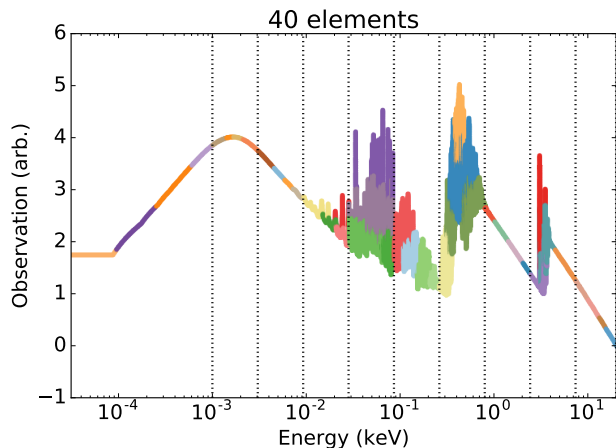


Fig. 5: Example spectrum from which the FEDS energy mesh is constructed. Markers with the same color correspond to energies that belong to the same energy element. Dotted lines correspond to coarse-group boundaries.

energy drives a shock through a fill gas within a tube. In these types of problems, radiation-driven wall-heating of the tube is an important phenomenon. We ignore the scattering cross section for these results.

Our spatially analytic characteristic begins with zero intensity in shocked argon⁵ of thickness 0.0277 cm at a density of 0.030 g/cc and temperature of 0.1 keV. The ray then passes through un-shocked (also called pre-shocked) argon of thickness 0.00416 cm, density of 0.0020 g/cc and temperature of 0.07 keV. It finally passes through polyimide plastic to a thickness of 0.0000361 cm at a density of 1.43 g/cc and a temperature of 0.025 keV. Figure 6 gives a graphical representation of this setup. The temperatures were chosen as representative from a time-dependent run with 20 groups [4]. The average number of bound electrons per ion for the shocked argon, unshocked argon, and plastic are 5.8, 6.0, and 2.7, respectively. Despite their similar average ionizations, the opacities of the two argon states are only moderately correlated (cf. Fig. 3).

We use a highly-resolved energy group structure with MG as the reference calculation. Our continuous-energy — often called "monochromatic" to denote a lack of averaging or interpolation — opacities were defined on a piecewise-uniform 14,900-point temperature-dependent energy grid [5]. We extrapolated these onto a thinned union grid using methods presented in [1]. Extrapolation was necessary because the original grid was based on E/T , meaning different temperatures had different minimum and maximum energies. While not fully spectroscopically resolved, the monochromatic energy grid was developed to ensure accuracy of integral metrics, such as reaction rates.

Figure 7 shows the reference absorption rate densities (ARDs, defined below) for the ray at the terminus of each material. The dotted lines show the ARDs for infinite material thicknesses. Figure 8 shows the reference intensity for the ray

⁵While the CRASH experiments used xenon, opacity availability forces us to use number-density-equivalent argon.

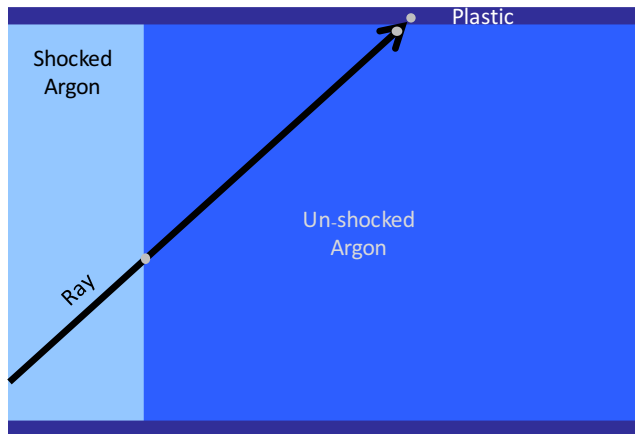


Fig. 6: Cartoon of our CRASH-like problem. We compute the intensity along a ray that begins in the shocked argon and ends in the plastic. Relative thicknesses are to scale. Gray dots indicate locations where the heating and absorption rate densities are computed, with the location of the dot in plastic at exaggerated depth.

at the terminus of each material with the dotted lines indicating the corresponding infinite-medium Planck distributions. Short optical depths at high energies in the plastic lead to imprinting of argon line structure on plastic ARD and intensity. Figure 8 (b) highlights this imprinting of upstream line structure on downstream intensities.

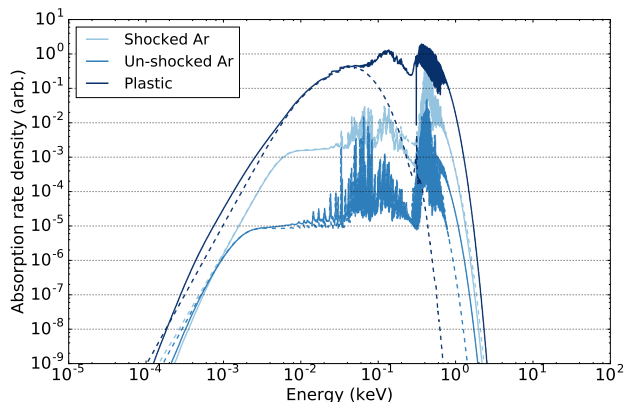
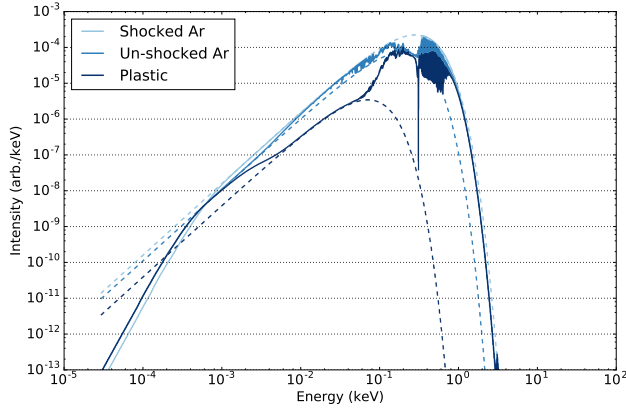
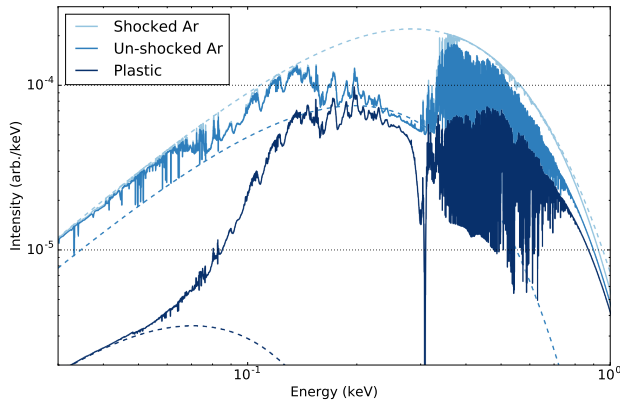


Fig. 7: Energy-dependent ARD as the ray exits each material in the CRASH-like problem (solid) and the infinite-medium values (dashed)

Our CRASH-like problem has thick and thin regions. Figure 9 shows that the optical depth (in mean-free-paths) of each material for our ray varies by orders of magnitude based on photon energy. Energy-independent depths were computed by averaging the optical depths in Fig. 9 using various weighting functions, including the reference intensity leaving the region, the most equilibrated of the intensities within the region. The different estimates of optical depth, given in Table I, differ radically due to the large range of magnitudes in the attenuation coefficients and the disparities among the various



(a) Full energy range



(b) Zoom

Fig. 8: Energy-dependent intensities as the ray exits each material in the CRASH-like problem (solid) and the infinite-medium Planck distributions (dashed)

weighting functions. The thickest estimate of the thickest material, shocked argon, had an average optical depth of 7 mfp along the direction of the ray, making our problem relatively thin compared to many high-energy-density physics applications that have orders of magnitude larger optical depths. The flat weighting emphasizes the contribution from the high-energy opacities and produces smaller averaged optical depths. The Planck weighting is known to be accurate for emission-dominated problems, while the Rosseland weighting performs well for wave-like problems near the EDL. The large percent differences in Table I show our CRASH-like problem fits neither of these regimes.

We compute three measures of error. The first is the relative error of the total heating rate density at the end of each material. The total heating rate density is defined as $\sum_e \sigma_{a,e}(s)[I_e(s) - B_e(s)]$, with s is the distance along our ray. The attenuation coefficient and Planckian are constant within a material region because temperature and density are constant. This metric relates to the internal energy deposition rate density, or heating, from the radiation to the material. The second relative error, taken at the same locations, is of the absorp-

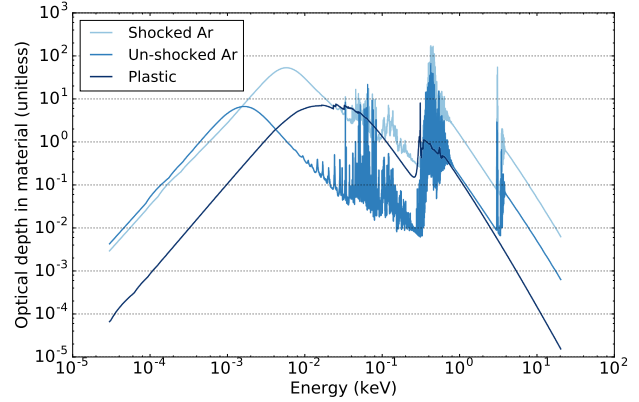


Fig. 9: Energy-dependent optical depths for each material in the CRASH-like problem

tion rate density (ARD), which is defined as $\sum_e \sigma_{a,e}(s)I_e(s)$. This metric does not have subtractive cancellation for energies and locations where the intensity is near equilibrium, making it more sensitive to accurate discretization of the opacity. This metric loosely relates to the momentum deposition rate density, which in the absence of scattering has a similar form in energy⁶, if not in angle. The final error is the opacity averaging error, which is a measure of the variation of the opacity within an element. The log of this error is defined as $\sqrt{\sum_e \sum_{f \in e} |\log_{10} \sigma_{ref.,f} - \log_{10} \sigma_e|^2 / N_{ref.}}$, where f is the fine-group index of the reference opacity and $N_{ref.}$ is the number of reference groups.⁷ The hierarchical agglomerative clustering algorithm used to compute the FEDS energy grid minimizes the L^2 norm of this error metric over all materials. Our opacity error is computed for each material separately.

Tables II - IV show three errors for various energy unknown counts using either FEDS or MG for our CRASH-like problem. For each result, the ten coarse groups listed above were used, with an equal number of energy unknowns per coarse group. Three quantities are given in these tables. The first are errors in the metrics for MG and FEDS. The second, in parentheses, gives the reduction in error compared to ten energy unknowns, with larger values denoting higher error reduction. These columns quantify convergence and, for N energy unknowns, would be equal to $N/10$ for first-order convergence in energy. The last, in square brackets, gives the ratio of MG error to FEDS error. Values greater than unity correspond to FEDS attaining lower error than MG.

Different basis functions tended to produce similar errors, with some notable exceptions. Errors using flat and Planck weightings were highly similar, with Planck weighting attaining lower errors for ARD in shocked argon (Table II) and flat weighting attaining lower errors in heating and ARD for plastic (Table IV). Figures 7 and 8 show the shocked argon to be

⁶The ARD is a relevant proxy for momentum rate density only when away from equilibrium. In the EDL, the radiation energy flux is proportional $1/\sigma_r(E)$, dividing out the $\sigma_r(E)$ used the momentum deposition rate.

⁷The first coarse group was not included in the opacity averaging error because, although the ratio of maximum to minimum opacity in that coarse group was large, the first coarse group also had the highest relative energy width and had negligible contribution to the solution or reaction rates.

TABLE I: Measures of thickness in optical depth for materials in the CRASH-like problem with various opacity weightings. Relative differences to intensity weighting are given in parentheses.

Material	Planck weighting		Rosseland weighting		Flat weighting		Intensity weighting
Shocked Ar	5.30	(-26%)	1.113	(-84%)	0.428	(-94%)	7.16
Un-shocked Ar	0.41	(6.5%)	0.022	(-94%)	0.042	(-89%)	0.38
Plastic	2.47	(370%)	0.666	(26%)	0.045	(-91%)	0.53

near equilibrium, where Planck weighting would be accurate. The plastic was sufficiently far from equilibrium that it was more accurate to assume no information in the weighting than to use the local Planckian. Rosseland-equivalent weighting attained low errors in heating rates and opacity variance but not ARD — except in the plastic, which had a smooth opacity. The ARD error from Rosseland weighting converges but is between 5 and 160 times larger for the argons than from flat or Planck weighting. As described above, ARD requires accurate treatment of large opacities, while heating is insensitive to large opacities because they equilibrate over small depths and cease to contribute to the heating. Rosseland weights against large opacities because of the opacity in its denominator.

MG was uneven in its error magnitudes and convergence rates. In the shocked argon (Table II), MG was able to achieve 5% heating errors with all three weightings and 160 unknowns. ARD errors of less than 5% were attainable using 20 elements with flat or Planck weighting. In the thin un-shocked argon, with its increased presence of lines, MG fared worse (Table III), obtaining 18% and 9.5% errors for heating and ARD with 320 groups for Planck or flat weighting. Opacity averaging errors were around a factor of two worse than for the shocked argon. While MG produced low opacity averaging errors in the plastic due to its smooth opacity (Table IV), heating and ARD errors were higher because they relied on accuracy in the upstream argons. Aside from Rosseland weighting at low unknown count, MG attained at best 10% error in heating and ARD in the plastic. These errors did not converge for the numbers of energy unknowns studied.

For the same number of unknowns, FEDS achieved lower errors than MG with few exceptions. The exceptions were at the lowest number of unknowns — where FEDS and MG both used elements equal to the coarse groups — for some cases at low unknown counts — where MG fortuitously achieved lower errors than at higher unknown counts — and for the opacity averaging error in plastic — whose opacity was less efficiently captured by the FEDS element structure that dedicated some unknowns to resolving the line structure in the argons. FEDS tended to converge at a faster rate than MG, doing better compared to MG at higher unknown counts, though for the shocked argon FEDS had the best error ratios around 40 - 80 groups for flat or Planck weighting. FEDS was able to achieve 5.7% error in heating using flat or Planck weighting in the shocked argon (Table II) with 40 elements, and 1.3% error in ARD with 20 elements. In the un-shocked argon (Table III), FEDS achieved 10% error in heating and ARD with flat or Planck weighting and 80 elements, with continuing convergence at higher unknown counts. In the plastic (Table IV), FEDS achieved 1.6% error in heating and ARD with

flat weighting and 40 groups, and 4.7% errors with Planck weighting and 80 groups, again with continuing convergence at higher unknown counts.

IV. CONCLUSIONS

In this research we have extended the Finite Element with Discontiguous Support (FEDS) method to thermal radiation transport (TRT) and tested it on a simplified high-energy density physics problem where wall heating is important. While TRT is challenging due to high-dimensional temperature-, density-, and material-dependences in the fine structure of the opacities, we were able to apply FEDS to this regime and our test showed convergence and low errors using 10 coarse groups and between 1 and 32 elements per coarse group. One interesting result is that resolving wall heating in our CRASH-like problem without relying on error cancellation required around 80 or more energy unknowns. This raises the question of required energy fidelity for TRT problems more generally, especially in regions far from material-radiation equilibrium.

Our CRASH-like problem, while not representative of all TRT problems, showed improved convergence and lower errors for FEDS compared to MG with the same number of unknowns in energy. With 160 unknowns and FEDS, we were able to achieve between 0.32% and 3.1% relative errors in heating rate and ARD in the plastic, depending on the weighting scheme used. For the same number of unknowns, MG had errors that were between 9.6% and 11%, a factor of 3 - 30 higher. For the same number of energy unknowns, opacity averaging errors, a measure of the unresolved variation of the opacity within an element, were between a factor of 1.9 and 2.1 lower for FEDS than MG in the shocked argon with its moderate line coverage, and between a factor of 3.3 and 3.8 lower in the un-shocked argon with its significant line coverage (cf. Figs. 1 and 2). For materials downstream of the line-blanketed un-shocked argon, FEDS continued to converge out to 320 elements, while MG stagnated for the reaction-rate metrics.

Overall, we found the advantage of FEDS over MG was associated with being downwind of a thin region that had both heavy line structure in its opacity and a temperature whose corresponding Planck overlapped with these lines. While further and more realistic tests are needed, these preliminary results indicate FEDS may provide both enhanced convergence and lowered error for the same amount of work as MG for problems with opacities that are line-dominated.

TABLE II: Errors in shocked argon using various basis functions to weight the opacities. Values in parentheses are ratios of errors of fewer to more energy unknowns. Values in brackets are ratios of MG error to FEDS error.

Weighting	Energy Unknowns	MG Error	MG Conv.	FEDS Error	FEDS Conv.	Ratio (MG/FEDS)
Heating Error						
Flat	10	0.296	(1.00)	0.296	(1.00)	[1.00]
	20	0.351	(0.85)	0.0415	(7.14)	[8.44]
	40	0.104	(2.84)	0.0574	(5.16)	[1.82]
	80	0.109	(2.72)	0.00846	(35.03)	[12.86]
	160	0.0412	(7.20)	0.0134	(22.14)	[3.07]
	320	0.0388	(7.65)	0.0128	(23.17)	[3.03]
Planck	10	0.308	(1.00)	0.308	(1.00)	[1.00]
	20	0.396	(0.78)	0.145	(2.12)	[2.73]
	40	0.119	(2.58)	0.0493	(6.25)	[2.42]
	80	0.111	(2.78)	0.0226	(13.67)	[4.92]
	160	0.0419	(7.36)	0.0174	(17.75)	[2.41]
	320	0.0388	(7.94)	0.0164	(18.83)	[2.37]
Rosseland	10	0.929	(1.00)	0.929	(1.00)	[1.00]
	20	0.447	(2.08)	0.486	(1.91)	[0.92]
	40	0.0324	(28.70)	0.1	(9.29)	[0.32]
	80	0.0244	(38.05)	0.0185	(50.35)	[1.32]
	160	0.0124	(75.16)	0.018	(51.63)	[0.69]
	320	0.00596	(155.85)	0.00539	(172.52)	[1.11]
ARD Error						
Flat	10	0.0866	(1.00)	0.0866	(1.00)	[1.00]
	20	0.0493	(1.76)	0.0134	(6.48)	[3.69]
	40	0.0224	(3.87)	0.00352	(24.57)	[6.35]
	80	0.00479	(18.09)	0.00138	(62.66)	[3.46]
	160	0.00401	(21.61)	0.00205	(42.30)	[1.96]
	320	0.0028	(30.95)	0.00189	(45.71)	[1.48]
Planck	10	0.0107	(1.00)	0.0107	(1.00)	[1.00]
	20	0.0138	(0.78)	0.00504	(2.12)	[2.73]
	40	0.00415	(2.58)	0.00171	(6.25)	[2.42]
	80	0.00386	(2.78)	0.000784	(13.67)	[4.92]
	160	0.00146	(7.36)	0.000604	(17.75)	[2.41]
	320	0.00135	(7.94)	0.000569	(18.83)	[2.37]
Rosseland	10	0.845	(1.00)	0.845	(1.00)	[1.00]
	20	0.706	(1.20)	0.452	(1.87)	[1.56]
	40	0.533	(1.59)	0.277	(3.06)	[1.93]
	80	0.334	(2.53)	0.22	(3.85)	[1.52]
	160	0.284	(2.98)	0.115	(7.37)	[2.47]
	320	0.249	(3.39)	0.0897	(9.43)	[2.78]
Opacity Averaging Error						
Flat	10	2.26	(1.00)	2.26	(1.00)	[1.00]
	20	2.3	(0.98)	1.26	(1.79)	[1.82]
	40	1.14	(1.97)	0.71	(3.18)	[1.61]
	80	0.874	(2.58)	0.511	(4.42)	[1.71]
	160	0.71	(3.18)	0.381	(5.93)	[1.87]
	320	0.611	(3.69)	0.292	(7.73)	[2.09]
Planck	10	2.36	(1.00)	2.36	(1.00)	[1.00]
	20	2.28	(1.04)	1.43	(1.66)	[1.60]
	40	1.18	(2.00)	0.709	(3.34)	[1.66]
	80	0.848	(2.79)	0.509	(4.65)	[1.67]
	160	0.727	(3.25)	0.381	(6.20)	[1.91]
	320	0.609	(3.88)	0.292	(8.09)	[2.08]
Rosseland	10	4.72	(1.00)	4.72	(1.00)	[1.00]
	20	4.46	(1.06)	1.74	(2.72)	[2.57]
	40	1.62	(2.91)	0.76	(6.21)	[2.13]
	80	1.11	(4.26)	0.53	(8.90)	[2.09]
	160	0.796	(5.93)	0.383	(12.32)	[2.08]
	320	0.667	(7.07)	0.298	(15.81)	[2.24]

TABLE III: Errors in un-shocked argon using various basis functions to weight the opacities.

Weighting	Energy Unknowns	MG Error	MG Conv.	FEDS Error	FEDS Conv.	Ratio (MG/FEDS)
Heating Error						
Flat	10	0.942	(1.00)	0.942	(1.00)	[1.00]
	20	0.835	(1.13)	0.212	(4.44)	[3.94]
	40	0.217	(4.34)	0.146	(6.45)	[1.49]
	80	0.239	(3.95)	0.104	(9.07)	[2.30]
	160	0.181	(5.21)	0.0519	(18.14)	[3.48]
	320	0.181	(5.20)	0.0221	(42.56)	[8.18]
Planck	10	0.996	(1.00)	0.996	(1.00)	[1.00]
	20	0.955	(1.04)	0.174	(5.71)	[5.47]
	40	0.283	(3.52)	0.107	(9.31)	[2.65]
	80	0.252	(3.95)	0.0862	(11.55)	[2.92]
	160	0.188	(5.29)	0.0506	(19.68)	[3.72]
	320	0.184	(5.43)	0.0235	(42.44)	[7.82]
Rosseland	10	0.85	(1.00)	0.85	(1.00)	[1.00]
	20	0.369	(2.30)	0.274	(3.10)	[1.35]
	40	0.0377	(22.52)	0.153	(5.56)	[0.25]
	80	0.031	(27.38)	0.0427	(19.92)	[0.73]
	160	0.0793	(10.72)	0.00181	(468.66)	[43.73]
	320	0.0888	(9.57)	0.00753	(112.78)	[11.79]
ARD Error						
Flat	10	0.463	(1.00)	0.463	(1.00)	[1.00]
	20	0.572	(0.81)	0.118	(3.93)	[4.86]
	40	0.142	(3.26)	0.0873	(5.31)	[1.63]
	80	0.128	(3.63)	0.0506	(9.15)	[2.52]
	160	0.0995	(4.66)	0.0259	(17.88)	[3.84]
	320	0.0951	(4.87)	0.0108	(42.82)	[8.79]
Planck	10	0.511	(1.00)	0.511	(1.00)	[1.00]
	20	0.489	(1.04)	0.0894	(5.71)	[5.47]
	40	0.145	(3.52)	0.0549	(9.31)	[2.65]
	80	0.129	(3.95)	0.0442	(11.55)	[2.92]
	160	0.0965	(5.29)	0.026	(19.68)	[3.72]
	320	0.0941	(5.43)	0.012	(42.43)	[7.82]
Rosseland	10	0.894	(1.00)	0.894	(1.00)	[1.00]
	20	0.613	(1.46)	0.479	(1.87)	[1.28]
	40	0.397	(2.25)	0.273	(3.27)	[1.45]
	80	0.334	(2.68)	0.197	(4.55)	[1.70]
	160	0.294	(3.04)	0.0942	(9.49)	[3.12]
	320	0.277	(3.23)	0.0663	(13.48)	[4.18]
Opacity Averaging Error						
Flat	10	3.3	(1.00)	3.3	(1.00)	[1.00]
	20	3.44	(0.96)	2.1	(1.57)	[1.64]
	40	1.98	(1.66)	0.963	(3.42)	[2.06]
	80	1.85	(1.78)	0.759	(4.35)	[2.44]
	160	1.71	(1.93)	0.513	(6.43)	[3.33]
	320	1.56	(2.11)	0.351	(9.40)	[4.46]
Planck	10	3.39	(1.00)	3.39	(1.00)	[1.00]
	20	3.22	(1.05)	2.29	(1.48)	[1.40]
	40	1.98	(1.71)	0.96	(3.54)	[2.07]
	80	1.83	(1.85)	0.787	(4.31)	[2.33]
	160	1.74	(1.96)	0.52	(6.52)	[3.33]
	320	1.57	(2.16)	0.353	(9.62)	[4.45]
Rosseland	10	15.8	(1.00)	15.8	(1.00)	[1.00]
	20	9.63	(1.64)	5.2	(3.04)	[1.85]
	40	2.84	(5.58)	1.13	(13.97)	[2.51]
	80	2.39	(6.63)	0.793	(19.96)	[3.01]
	160	2.02	(7.82)	0.537	(29.48)	[3.77]
	320	1.85	(8.58)	0.355	(44.56)	[5.19]

TABLE IV: Errors in plastic using various basis functions to weight the opacities.

Weighting	Energy Unknowns	MG Error	MG Convg.	FEDS Error	FEDS Convg.	Ratio (MG/FEDS)
Heating Error						
Flat	10	0.197	(1.00)	0.197	(1.00)	[1.00]
	20	0.0426	(4.63)	0.135	(1.46)	[0.31]
	40	0.107	(1.84)	0.0128	(15.42)	[8.36]
	80	0.102	(1.94)	0.0156	(12.68)	[6.54]
	160	0.103	(1.91)	0.00321	(61.53)	[32.21]
	320	0.108	(1.83)	0.000705	(279.87)	[153.02]
Planck	10	0.237	(1.00)	0.237	(1.00)	[1.00]
	20	0.14	(1.69)	0.227	(1.04)	[0.62]
	40	0.0839	(2.82)	0.137	(1.73)	[0.61]
	80	0.0938	(2.53)	0.0474	(5.00)	[1.98]
	160	0.102	(2.33)	0.0147	(16.08)	[6.92]
	320	0.107	(2.22)	0.00938	(25.24)	[11.37]
Rosseland	10	0.0296	(1.00)	0.0296	(1.00)	[1.00]
	20	0.0632	(0.47)	0.00422	(7.02)	[14.98]
	40	0.197	(0.15)	0.194	(0.15)	[1.02]
	80	0.145	(0.20)	0.0993	(0.30)	[1.46]
	160	0.11	(0.27)	0.0312	(0.95)	[3.53]
	320	0.0971	(0.31)	0.0155	(1.91)	[6.25]
ARD Error						
Flat	10	0.183	(1.00)	0.183	(1.00)	[1.00]
	20	0.0393	(4.66)	0.128	(1.43)	[0.31]
	40	0.101	(1.82)	0.0128	(14.25)	[7.83]
	80	0.0956	(1.92)	0.0143	(12.79)	[6.68]
	160	0.097	(1.89)	0.00339	(53.98)	[28.58]
	320	0.101	(1.81)	0.000785	(233.25)	[129.00]
Planck	10	0.222	(1.00)	0.222	(1.00)	[1.00]
	20	0.131	(1.69)	0.213	(1.04)	[0.62]
	40	0.0788	(2.82)	0.128	(1.73)	[0.61]
	80	0.088	(2.53)	0.0445	(5.00)	[1.98]
	160	0.0956	(2.33)	0.0138	(16.08)	[6.92]
	320	0.1	(2.22)	0.00881	(25.24)	[11.37]
Rosseland	10	0.0147	(1.00)	0.0147	(1.00)	[1.00]
	20	0.0544	(0.27)	0.0141	(1.04)	[3.86]
	40	0.183	(0.08)	0.177	(0.08)	[1.04]
	80	0.136	(0.11)	0.0912	(0.16)	[1.49]
	160	0.103	(0.14)	0.028	(0.53)	[3.69]
	320	0.0911	(0.16)	0.0141	(1.04)	[6.48]
Opacity Averaging Error						
Flat	10	0.623	(1.00)	0.623	(1.00)	[1.00]
	20	0.378	(1.65)	0.501	(1.24)	[0.75]
	40	0.27	(2.31)	0.437	(1.43)	[0.62]
	80	0.203	(3.07)	0.243	(2.56)	[0.83]
	160	0.152	(4.10)	0.154	(4.04)	[0.99]
	320	0.0852	(7.31)	0.108	(5.78)	[0.79]
Planck	10	0.698	(1.00)	0.698	(1.00)	[1.00]
	20	0.49	(1.43)	0.547	(1.28)	[0.90]
	40	0.299	(2.34)	0.618	(1.13)	[0.48]
	80	0.218	(3.20)	0.307	(2.27)	[0.71]
	160	0.159	(4.40)	0.177	(3.95)	[0.90]
	320	0.0847	(8.25)	0.12	(5.82)	[0.71]
Rosseland	10	1.19	(1.00)	1.19	(1.00)	[1.00]
	20	0.934	(1.28)	0.812	(1.47)	[1.15]
	40	0.413	(2.89)	0.629	(1.90)	[0.66]
	80	0.208	(5.73)	0.292	(4.09)	[0.71]
	160	0.131	(9.09)	0.168	(7.12)	[0.78]
	320	0.0721	(16.55)	0.117	(10.17)	[0.61]

V. FUTURE WORK

The current work showed first steps toward TRT using FEDS. Further studies are needed to quantify performance on a wider range of problems, especially for thick, diffusive problems and problems that involve many temperature and density states. When studying these problems, the involved researchers may wish to employ more metrics than heating, absorption rate densities, total intensities, and within-element opacity variances.

There are two important hurdles to be overcome before FEDS can be used with TRT or radiation hydrodynamics (RH) generally. First, it is unlikely that we will be able to compute efficient global energy element definitions in the general case of many temperature and density states. This can be seen by extrapolating Fig. 3, which compares two temperature-density points, to the full temperature-density space for one material, then for several materials. The line structure is insufficiently correlated to allow efficient discretization using few energy unknowns. MG shares this challenge of efficiently discretizing in energy with few unknowns, especially when resolution of line structure in part or all of the energy domain is required. One path forward would be to define several independent sets of element boundaries. Temperatures, densities, and materials with different line structure would have different element definitions. Discrete-ordinate sweeping or Monte Carlo particle tracking could still be used, but intensities/particles within a coarse group ought to be remapped when they travel to a cell with a different element structure.

The other major challenge is material motion. Opacities are defined in the co-moving frame, a non-inertial frame where the material is locally at rest. Advection is simple in the laboratory frame, but opacities in this frame depend on material velocity and particle direction. For our MG, in which we used groups equally spaced over the log of photon energy, the opacity discrepancy is less important because the relative group widths are often wide compared to the velocity-induced relative shifts in energy between lab and co-moving frame. FEDS has energy elements that are composed of contiguous subelements, which are on the order of line widths. Even small velocity-induced shifts are large relative to line widths: for this CRASH-like problem, 10% of the FEDS subelements in the energy grid had relative spacings of less than $\sim 3\text{-}4 \times 10^{-5}$. Material motion with speed $\sim 3 \times 10^{-5}c$, which is around 10^6 cm/s or 10 km/s ($\mu\text{m/ns}$), will induce red-/blue-shifts of this magnitude. This implies FEDS intensities will see intensity smearing of elements whose subelements resolve line widths when the physical problem has velocity gradients larger than total attenuation coefficients multiplied a few $10^{-5}c$ or so. It will be important to quantify the effect of this smearing for realistic problems. We are developing methods to handle material motion while still allowing S_N sweeping by using intensity mappings that couple all groups and account for red- and blue-shifts between cells. When particle tracking is used in Monte Carlo methods, sampling of columns of this map can be used to Doppler shift the particles.

APPENDIX: ROSSELAND WEIGHTING AND MIXTURES

In this appendix, we discuss the properties of Rosseland-equivalent basis functions, defined in Eq. (3a). The total attenuation coefficient weighted with $b_{e,R}$ is indeed the Rosseland average over the element:

$$\begin{aligned} \sigma_{t,R,e}(\mathbf{r}, t) &= \frac{\int_0^\infty dE b_{e,R}(\mathbf{r}, E, t) \sigma_t(T_m(\mathbf{r}, t), \rho_m(\mathbf{r}, t), E)}{\int_0^\infty dE b_{e,R}(\mathbf{r}, E, t)} \\ &= \frac{\int_{\Delta E_e} \frac{\partial B}{\partial T}}{\int_{\Delta E_e} dE \frac{\partial B}{\partial T} \frac{1}{\sigma_t}}. \end{aligned} \quad (\text{A.1})$$

Further, this definition of the Rosseland-equivalent weighting naturally extends to produce consistently weighted partial attenuation coefficients. These partial inverse mean-free paths obey $\sigma_{t,R,e} = \sigma_{a,R,e} + \sigma_{s,R,e}$. This relationship would not hold were $\sigma_{a,e}$ to be defined as $\int_{\Delta E_e} dE (\partial B / \partial T) / \int_{\Delta E_e} dE (\partial B / \partial T) (1 / \sigma_a)$.

In practice, the Rosseland-equivalent basis function in Eq. (3a) is not used for atomic mixtures⁸ of multiple materials because the opacity in Eq. (3a) would be the energy-dependent opacity for the mixture, viz. $\kappa_t(E) = \sum_i f_i^M \kappa_i(\rho_i, T, E)$, with i the index of materials within the cell, f_i^M the mass fractions, and ρ_i the partial densities.⁹ It is infeasible to store the MG or FEDS mixture opacity for all possible combinations of constituents (*i.e.*, all combinations of ρ_i and T). It is also infeasible to store the temperature- and density-dependent, *energy-dependent* opacities for each material and mix them on-the-fly to produce the proper Rosseland-weighted average of the mixture. Notice this latter problem does not arise for Planck- and flat-weighted opacities because the weighting functions do not depend on the opacity, so each material may be preprocessed independently and the discretized opacities mixed arithmetically at run-time.

The work-around for Rosseland-weighted opacities of atomic mixtures is to preprocess MG or FEDS opacities for pure materials and approximate the MG / FEDS opacity of the mixture as the arithmetic or harmonic mean of the constituent MG / FEDS opacities weighted by their mass fractions. See [6] for further discussion of opacity mixing.

This work-around leads to two undesired consequences. The first is that the wrong weighting is used, with the single-material energy-dependent opacities instead of the mixture opacity used in the weighting functions. This can be significant because the former does not take self-shielding of opacities into account, where one large opacity can shield the weighting function from the line structure of another opacity.

The other difficulty is that using multiple weighting functions within a cell leads to undefined $I(E)$, though I_e and hence reaction rates are still well-defined because κ_e is well defined for each mixture. Multi-material problems are beyond the scope of this paper and all of our spatial regions contain single materials. All of the challenges associated with multi-material problems occur for both MG and FEDS.

⁸Other types of mixtures may require different treatments.

⁹For atomic mixtures, $\rho_i = f_i^M \rho$. This does not hold if components occupy disparate volumes.

APPENDIX: SIMILARITIES AND DIFFERENCES BETWEEN THE FEDS AND MG TRT EQUATIONS

In this appendix, we discuss differences between the FEDS and MG methods related to their implementation in TRT codes. The FEDS time-discretized TRT equations in Eq. (8a) are indistinguishable from the MG time-discretized TRT equations apart from one important difference. With FEDS, integrals of B and $\partial B/\partial T$ are over ΔE_e , which is a discontinuous set of energy intervals. Each individual interval comprises a subelement and is contiguous. The number of these intervals is often proportional to the number of lines within an element, so exact calculations of B_e and $\partial B_e/\partial T$, while straightforward, may be expensive. For our CRASH-like problem, the ratio of the number of intervals to elements for FEDS ranged from 13 to 30, with higher ratios for lower numbers of elements. In many codes, these integrals are computed only once per cell per timestep and so the cost may be amortized if many transport/diffusion iterations or particles are used within the timestep. Cheaper, approximate alternatives are also possible.

It is straightforward to include energy-altering Compton scattering in the TRT equations and solvers with FEDS. The scattering kernel, stored for each incident element, exiting element, and Legendre moment, can be precomputed over the elements and subsequently used in an identical manner to the scattering kernel in NT [1].

While FEDS can produce elements with large opacities that correspond to line peaks, the $1/E^3$ energy dependence of the free-free opacity at low-to-mid photon energies (cf. Fig. 1) ensures MG will also produce groups with large opacities. It is therefore expected that FEDS can use the same spatial / temporal / angular discretization resolutions as MG.

The right-hand side of the time-discretized FEDS TRT equation can become negative for some elements for sufficiently large timesteps and fine elements. This occurs because the energy shape of $B(E)$ is not the same as that of $\partial B/\partial T(E)$. While this can occur for both FEDS and MG, one may expect it to occur more easily for FEDS, as some elements cover small energy widths and the maximum pointwise difference between the normalized Planckian and its temperature derivative will always be larger than differences of integrals. It is unclear how often these negativities might occur or what their effect would be when they do occur.

ACKNOWLEDGMENTS

Los Alamos Report LA-UR-17-20825. Funded by the Department of Energy at Los Alamos National Laboratory under contract DE-AC52-06NA25396.

REFERENCES

1. A. T. TILL, *Finite Elements with Discontiguous Support for Energy Discretization in Particle Transport*, Ph.D. thesis, Texas A&M University, College Station, TX (December 2015).
2. A. T. TILL, M. HANUŠ, J. E. MOREL, and M. L. ADAMS, "Comparisons of the Finite-Element-with-Discontiguous-Support Method to Continuous-Energy Monte Carlo for Pin-Cell Problems," in "International Conference on the Physics of Reactors (PHYSOR) - Unifying Theory and Experiments in the 21st Century," American Nuclear Society, Sun Valley, Idaho, USA (May 2016).
3. D. M. MIHALAS and B. MIHALAS, *Foundations of Radiation Hydrodynamics*, Dover Publications, Inc., Mineola, New York (1999).
4. R. P. DRAKE, M. L. ADAMS, J. P. HOLLOWAY, K. G. POWELL, Q. F. STOUT, ET AL., "Final Report," Tech. Rep. DE-FC52-08NA28616, Center for Radiative Shock Hydrodynamics, Atmospheric, Oceanic, and Space Sciences, University of Michigan (April 2014).
5. L. H. FREY, W. EVEN, D. J. WHALEN, C. L. FRYER, A. L. HUNGERFORD, C. J. FONTES, and J. COLGAN, "The Los Alamos Supernova Light-curve Project: Computational Methods," *The Astrophysical Journal Supplement Series*, **204**, 2, 16 (2013).
6. C. N. ZEEB and C. J. FONTES, "A Study of the TOPS and RAGE Methods for Calculating Mixed Opacities," Tech. Rep. LA-UR-06-0882, Los Alamos National Laboratory (2006).